Electrical conductivity evolution of non-saturated carbonate rocks during deformation up to failure

Laurence Jouniaux,[1] Maria Zamora[2] and Thierry Reuschlé[3]

[1]*Institut de Physique du Globe de Strasbourg, CNRS UMR7516, 5, rue René Descartes, 67084 Strasbourg Cedex, France.*
E-mail: Laurence.Jouniaux@eost.u-strasbg.fr
[2]*Institut de Physique du Globe de Paris, France*
[3]*Institut de Physique du Globe de Strasbourg, CNRS UMR7516, France*

SUMMARY

We present electrical conductivity measurements (at a fixed frequency of 1 kHz) performed on three directions on limestone samples from the quarry of Meriel, during uniaxial tests of deformation up to failure. Samples were saturated from 100 to 80 per cent by drainage. The samples showed brittle fracture with Young's modulus in the range 10–13 MPa. Formation factor (sample resistivity divided by water resistivity) values range between 2 and 4. In saturated conditions the electrical measurements reflect the initial rock compaction, followed by dilatancy due to new axial cracks formation and finally crack coalescence, fracture localization and failure. The conductivity increase is related to the crack porosity Φ_c, which starts to increase at relatively low stress (31 per cent of strength). The magnitude of the electrical conductivity variation is 1–4 per cent of the initial value. We show that when saturation is decreased the conductivity increase occurs earlier during the deformation process, from 68 to 17 per cent of strength for 100 to 80 per cent of water saturation, respectively, so that the decrease in conductivity at low stress is less and less present. The induced relative rock conductivity variation in non-saturated and undrained conditions is the result of two competing effects: the relative porosity variation and the relative saturation variation during the deformation process. During compaction the electrical conductivity can show either a small decrease or a small increase; since the size of the partially saturated pores and cracks is reduced, the water occupies a larger percentage of the pore space, and then conductivity can be increased at this stage. We show a *continuous* increase of the conductivity both during the compaction and the dilatancy phases when the initial saturation is about 80–85 per cent. Finally a power law is shown between conductivity and stress, so that the relative electrical conductivity increase is larger as one goes along the compression process.

Just before failure, at 90–95 per cent of strength, the rate increase in horizontal conductivity drops, so that the anisotropy between axial and radial conductivity is about 0.5–2 per cent. At failure a drastic increase of this anisotropy can be seen, up to 5–6 per cent (CME21, CME24 and CME13 samples).

Key words: deformation, electrical anisotropy, electrical conductivity, fluids in rocks, laboratory measurements, rock fracture.

GJI Volcanology, geothermics, fluids and rocks

INTRODUCTION

Electrical resistivity can be used in geophysics to investigate the structure or the deformation of the crust (Henry *et al.* 2003; Le Pennec *et al.* 2001; Jouniaux *et al.* 1999; Pezard 1990). Since the electrical resistivity is related to mechanical properties (Glover *et al.* 2000; David *et al.* 1999; Bernabé 1986, 1995; Jouniaux *et al.* 1994), it can be used to detect fracture (Nover *et al.* 2000), or used for *in situ* stress determination (Cornet *et al.* 2003). The electrical conductivity is a combination of electrolytic conduction for the fluid-filled fractures and surface conduction for conductive alteration minerals, and depends on the degree of water saturation of the rock (Guichet *et al.* 2003). Therefore, it is also used to investigate the migration of fluids through crustal rocks, and to image active fault zones up to 10 km depth (Eberhart-Philipps *et al.* 1995).

Electrical properties of rocks have been studied in an attempt to find a physical basis for earthquake prediction. Changes in complex resistivity during laboratory creep experiments have suggested that it may be possible to identify earthquake nucleation regions through the use of standard electrical remote sensing techniques

(Lockner & Byerlee 1986). Changes in rock conductivity (DC or low-frequency measurements) under deformation up to failure in triaxial experiments have been measured in laboratory and showed first a decrease in conductivity at low stresses, and then an increase in conductivity when stresses are further increased (Brace & Orange 1968; Brace 1975; Jouniaux *et al.* 1992; Glover *et al.* 1997). The rate of conductivity increase was shown to be larger when water was flowing through the sample (Jouniaux *et al.* 1992). Some of these experimental results were discussed in conjunction with the dilatancy–diffusion model to interpret the field observations of pre-seismic changes in crustal resistivity (Scholz *et al.* 1973; Brace 1975). However, as noted sometime ago, many negative field observations have challenged the dilatancy–diffusion model (Takano *et al.* 1993).

Most of the previous experimental studies have focused on the resistivity changes under saturated conditions, which may not be representative of the shallow crust. Indeed, as a result of the magnetotelluric studies, it is well established that the upper crust is often anomalously resistive in comparison to the lower crust. This transformation occurs at depth of 13 to 20 km and is characterized by a decrease in resistivity of 1–3 orders of magnitude. The transition from high to low resistivity correlates with crustal temperature of about 400°C (Hyndman & Hyndman 1968; Hyndman & Shearer 1989; Marquis & Hyndman 1992; Thouret & Marquis 1994). An explanation for this anomalously resistive upper crust arises from the behaviour of fluids in the H_2O-CO_2 system. When a H_2O-CO_2 solution cools to temperature of 300°–400°C, a CO_2-rich phase will begin to separate from the aqueous solution (Nesbitt 1993). The resistivity of this CO_2-rich phase should be several orders of magnitude larger than the remaining aqueous solution (Olhoeft 1981). This may be especially effective in the upper brittle crust where permeability is largely a product of a few, relatively large fractures (Brace 1980). Consequently, even though fractures in the upper crust are probably largely saturated with a moderately conductive aqueous solution, the upper crust may be anomalously resistive due to the insulating properties of discrete CO_2-rich bubbles passing through the system (Nesbitt 1993). This leads to the conclusion that we need to know the behaviour of the electrical conductivity of rocks during deformation in non-saturated and non-drained conditions.

When the rock is not fully saturated the conductivity increases throughout the compaction (in uniaxial experiments: Parkhomenko & Bondarenko 1960; Yamazaki 1965, 1966), and the amplitude of conductivity increase drops when the saturation is increased (Yamazaki 1966). To have a better understanding of the rock structure evolution during deformation up to failure, and to track some precursory changes before rupture, we have focused on measurements of electrical properties of rock during deformation, and particularly the electrical anisotropy which has not been measured in previous studies. Since the electrical conductivity is related to the water content and to the porous structure, specially crack connectivity, it can reflect the evolution of the rock structure during deformation.

It is usually accepted that faulting in compressive brittle fracture is induced by coalescence of microcracks formed prior to faulting, these microcracks being randomly distributed and subparallel to the maximum compressive stress (Brace *et al.* 1966), and the coalescence occurring near the peak stress. During the linear part of volumetric strain–stress evolution the minerals distort elastically and grains or part of grains shift slightly under the applied stress and slide relative to each another (Brace *et al.* 1966). New cracks appear at pre-existing intergranular boundaries at the onset of dilatancy, and then at 50–75 per cent of peak stress new transgranular

cracks appear (Tapponier & Brace 1976; Fonseka *et al.* 1985). Small cracks grow steadily up to their coalescence leading to a macroscopic instability (Ashby & Sammis 1990). At later stages of deformation extensive crushing of particles into fine-grained gouge becomes important (Wong 1982).

Electrical data obtained during uniaxial compression tests reflect the initial rock compaction, followed by dilatancy due to new axial crack formation and finally crack coalescence, fracture localization and failure. We present the results of uniaxial compression tests run on limestone samples partially and fully saturated with water. This is the first time, in our knowledge, that the electrical anisotropy is quantified during deformation, since electrical measurements have been performed in three directions. Moreover, in non-saturated conditions, unlike previous studies focused on very low saturations, we performed measurements at relatively high water saturation such as 80–100 per cent, which is more representative of the shallow crust.

EXPERIMENTAL PROCEDURE

The studied samples come from the quarry of Meriel, France (Jouniaux *et al.* 1996; Morat & Le Mouël 1992; Morat *et al.* 1992). Meriel limestone is a bioclastic Lutetian limestone. The thin section of this limestone is shown in Fig. 1. The sample was impregnated with blue epoxy resin to reveal the pore spaces and cracks. The rock is not homogeneous since some isolated large pores can be present. The grains and pores are aligned in the bedding plane (the *X* direction). The porosity of studied samples, measured by triple weight, varies from 35.4 to 37.6 per cent (Table 1). Measurements carried out on
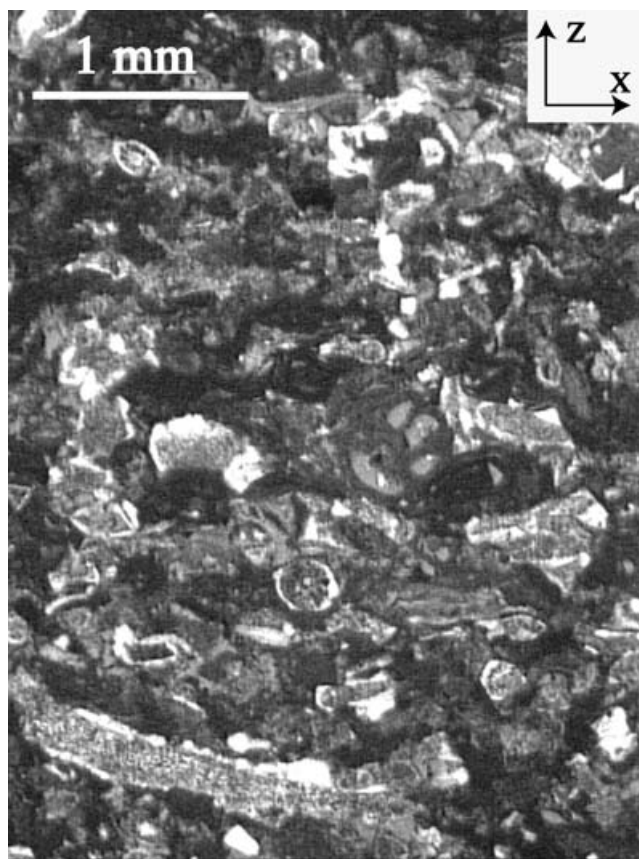

Figure 1. Thin section of Meriel limestone. The porous network is represented by blue epoxy.

Table 1. Porosity, water saturation, Young's modulus (E), peak stress, strain at peak stress, initial rock conductivity values, and water conductivity, for the studied samples.

	CME21	CME22	CME24	CME23	CME13	CME32
Porosity (per cent)	36.1	37.1	36.3	37.2	35.4	37.6
Water saturation (per cent)	100	95	91	87.6	85	80
E (MPa)	10.5	11.8	12.0	11.3	13.5	12.2
Peak stress (MPa)	4.0	4.5	4.1	4.5	4.9	4.7
Strain at peak stress (per cent)	0.68	0.63	0.86	0.70	0.69	0.63
σ_{0x} (S m^{-1})	0.28	0.26	0.25	0.24	0.22	0.25
σ_{0y} (S m^{-1})	0.28	0.27	0.26	0.28	0.22	0.25
σ_{0z} (S m^{-1})	0.52	0.53	0.44	0.48	0.40	0.41
σ_{f} (S m^{-1})	1.027	1.008	1.008	1.008	0.967	0.994

some samples taken beside our samples show that air permeability (measured by the constant flow technique) ranges from 74 to 374 × 10^{-15} m^2 (Jouniaux *et al.* 1996), and the access radii distribution shows peaks at 16 and 0.15 μm. These carbonate rocks have been chosen for their high porosities, so that the expected electrical conductivity variation induced by the deformation should be a low one compared to the amplitude variation expected for low-porosity rocks. For this study six parallelepedic (50 × 50 × 100 mm) samples were cut in the same block of rock. The rectangular geometry was chosen because it is more convenient for electrical anisotropy measurements and for further studies using acoustic sensors.

Samples were saturated under vacuum with salted (0.1 M NaCl) water (water conductivity was measured by a WTW LF330 conductivimeter and is ∼1 S m^{-1}, see Table 1), at six saturation levels ranging from 100 to 80 per cent. The electrical conductivity of the water is thought to be homogeneous inside the sample once it is saturated. Partial water saturation S_w was achieved by drainage of the sample, that is by drying the sample using a vacuum pump and placing it in a dessicator during 24 hr. The weight of the sample was measured to deduce the water saturation, the weight being measured before and after runs.

Samples were deformed up to failure under uniaxial compression at strain rate 3.5 to 6 × 10^{-7} s^{-1}. Typical experiment lasted 4–5 hr. Loading stress was increased in small steps and stress was held at 19 to 23 levels for periods of time 10–20 min to collect electrical data. The loading force and the axial displacement were measured, leading us to deduce the axial stress and the axial strain. The horizontal strains were not measured, so that the volumic deformation of the rock was not monitored.

Conductivity of the sample (a scheme of the sample is shown in Fig. 2) was measured in three directions (horizontal: x, y; axial or vertical: z) by a two-electrodes technique at a frequency of 1 kHz, using an HP impedance bridge. Electrodes consisted in silver paint on each surface. Impedance response of the sample at frequencies between 100 Hz and 20 kHz showed a quasi-pure resistance with no capacitive effect (angle of the impedance is 0.08° to 1°) and a fixed frequency of 1kHz was chosen for our measurements during deformation because it is often the frequency at which the out-of-phase conductivity is minimized. Measurements at a fixed frequency 1 kHz were, therefore, performed for each step in axial stress. It allows us to compare our measurements to other available data (Jouniaux *et al.* 1992; Glover *et al.* 1997). The application of an electrical field gives rise to different physical and physico-chemical processes both in the bulk and on the interfaces of components (Knight & Endres 1990). Since the water used showed a conductivity of about 1 S m^{-1}, and since the used frequency is 1 kHz, it is thought that we are in the regime where the conductivity is dominated by volumic conductiv-
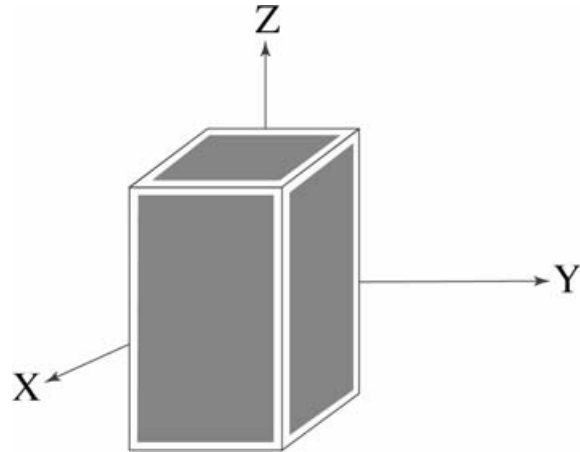
Figure 2. Scheme of the sample.

ity through water in pores and cracks and that surface conductivity is negligible. That is why the internal surface to volume ratio of the pores, which controls the relative importance of surface conduction processes in porous rocks (David *et al.* 1993) was not measured.

By measuring the electrical potential in one direction (x, y, or z) when a parallel current flows through a cross section of a sample, the impedancemeter measures the complex impedance Z of the sample, and the angle θ. The resistance R of the sample is deduced as $Z \cos(\theta)$. The conductivity of the sample is then calculated as $\sigma = (L/RS)$ where L is the length of the sample, and S is the section area. Therefore, the error on the rock conductivity is the sum of the errors on the measured resistance, the measured length, and the calculated section, and is ±0.9 per cent. Anisotropy of conductivity between x, y, and z direction has been calculated as followed: $\sigma_{xz} = (\sigma_z - \sigma_x)/\sigma_x$, and its relative variation has been plotted. Note that experiments are performed in undrained regime.

Typical resistance measurements were of the order of 65 to 81 ohm in horizontal directions, and of 140 to 181 ohm in the axial direction, which lead to resistivity values of 3.6–4.5 to 1.9–2.5 ohm m. The initial values of rock conductivities from 0.2 to 0.5 S m^{-1} are given in Table 1.

RESULTS

Since the sample is shortened during the axial compression test, its strain is the axial displacement measured by the press divided by the initial length of the sample. The axial stress is the loading force divided by the cross section of the sample, and the strength of the sample is the axial stress at failure.
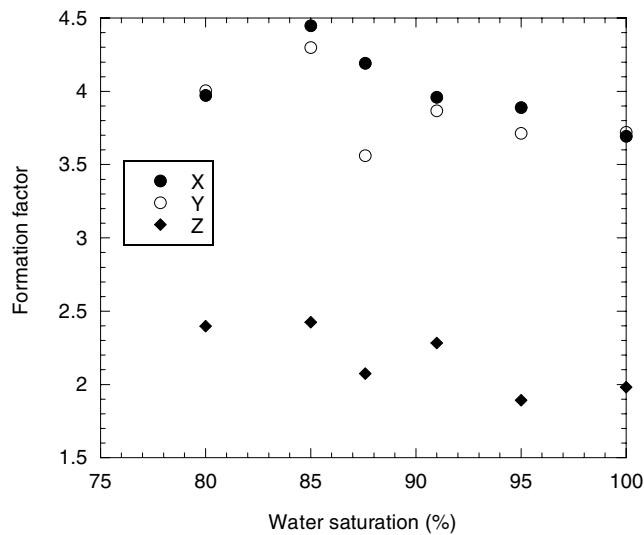
Figure 3. Initial formation factor in the three directions *X*, *Y* and *Z* versus water saturation of the samples.

Mechanical behaviour

Samples have been deformed up to 0.6–0.9 per cent in axial strain. They showed brittle axial fracture, the maximum stress ranged from 4.1 to 4.9 MPa, and Young's modulus, obtained in the linear part of the curve, was 10–13 MPa (Table 1).

Electrical behaviour

Initial formation factors (water conductivity divided by rock conductivity) are 3.5–4.5 in horizontal directions and 1.9–2.4 in the axial direction (consistent with Jouniaux *et al.* 1996), showing that the samples are about twice more conductive in the axial direction than in the horizontal plane. Since the water conductivity σ_f is about 1 S m^{-1}, the initial value of rock conductivities are between 0.2 and 0.5 S m^{-1}. Initial formation factors F_z, F_x, F_y have been plotted versus saturation (Fig. 3) and show a light decrease with increasing saturation.

Variations of the rock conductivity in *X*, *Y* and *Z* directions and variations of the anisotropy σ_{xy}, σ_{zx}, and σ_{zy} during the experimental tests have been plotted in Fig. 4. The magnitude of variation is about 2–4 per cent of the initial rock conductivity value.

We now describe the behaviour of the electrical conductivity of the six studied samples during the compression tests up to failure.

Sample CME21 was fully saturated and its porosity was 36.1 per cent. The electrical conductivities first decrease. At 73 per cent
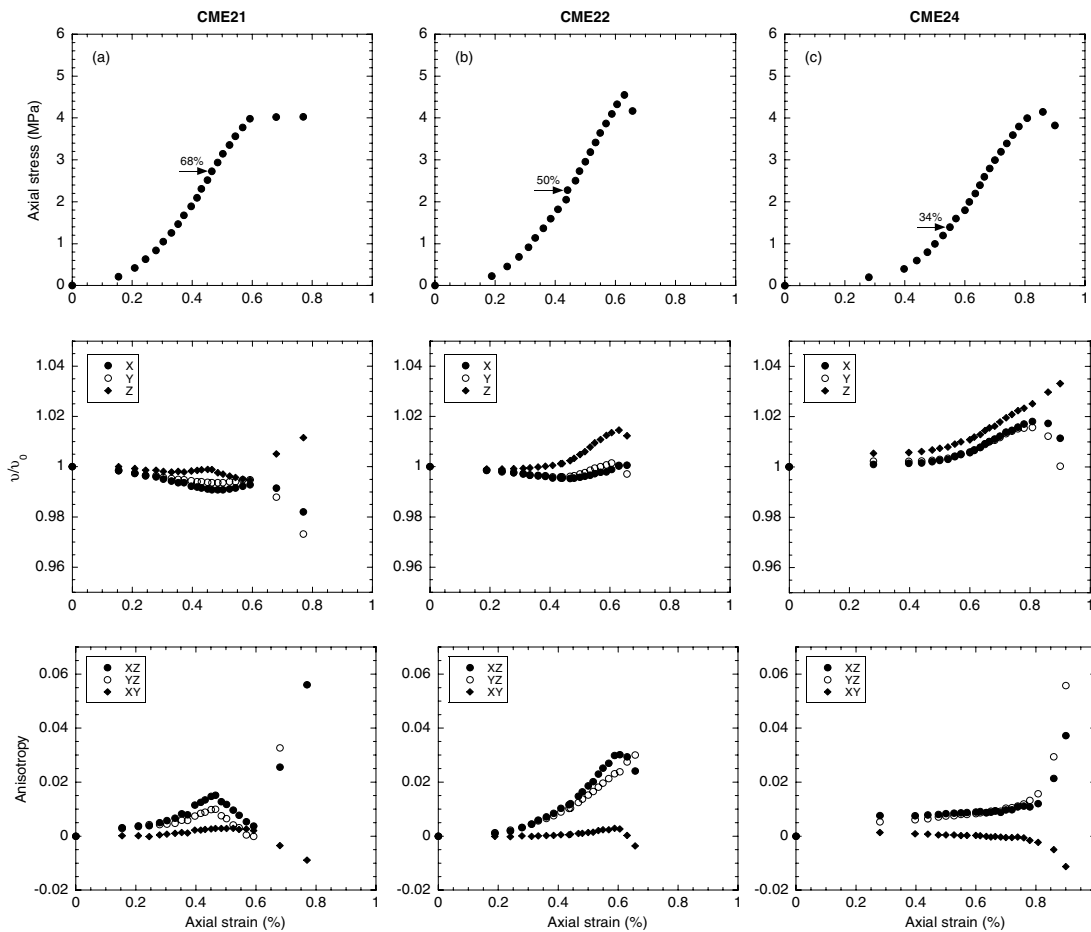

Figure 4. Axial stress, rock conductivity, and electrical anisotropy versus axial strain. 4a: CME21 sample; 4b: CME22 sample; 4c: CME24 sample; 4d: CME23 sample; 4e: CME13 sample and 4f: CME32 sample.
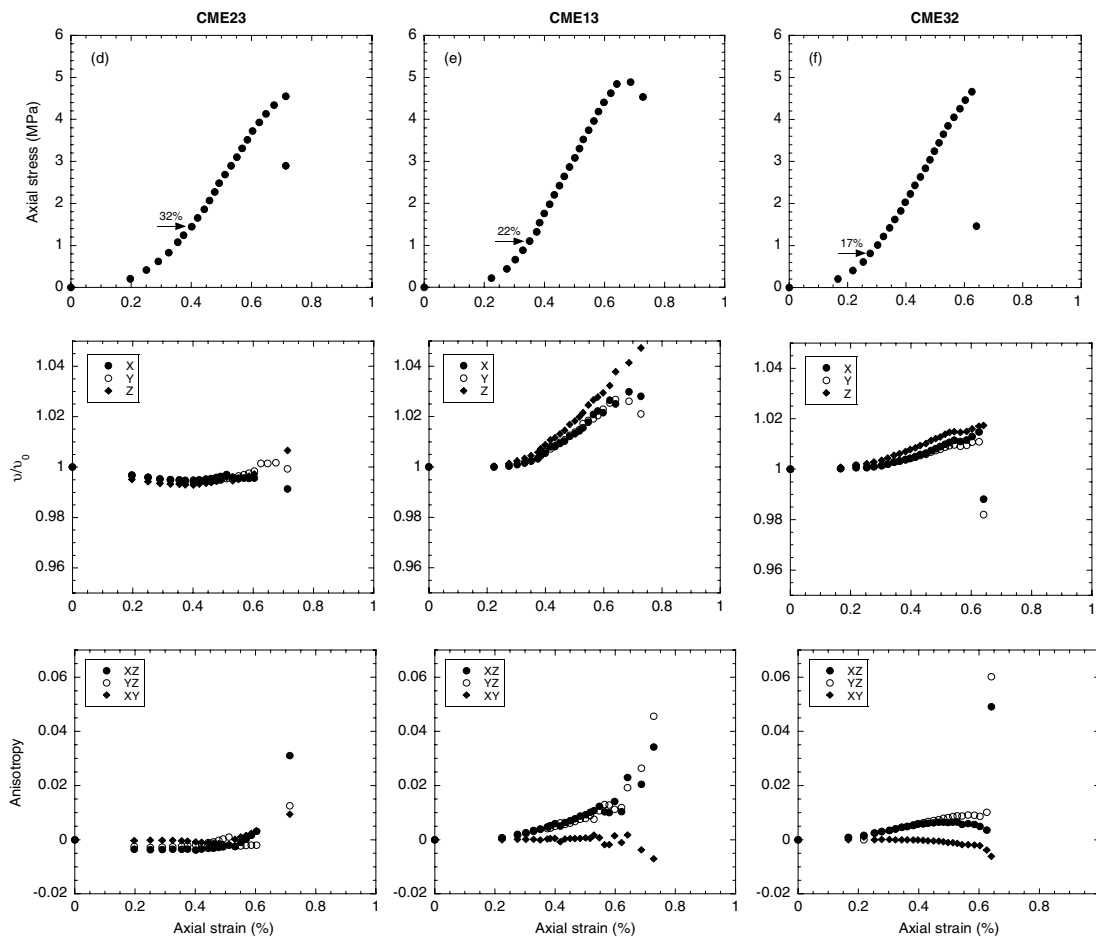
Figure 4. (*Continued.*)

of the strength the horizontal conductivities increase up to failure, the total variation being about 1 per cent. The axial conductivity tends to increase at low stress (37 per cent of strength), but then decreases well before failure (68 per cent of strength). At failure the axial conductivity increases by 2 per cent, whereas the horizontal conductivities decrease by 1–2 per cent, σ_x decreasing less than σ_y (Fig. 4a).

Sample CME22 was saturated at 95 per cent. The horizontal conductivities decrease by 0.5 up to 55 per cent of strength, and then increase by 0.5 per cent up to failure. The axial conductivity increases slowly at low stresses, and then increases more rapidly by 1.5 from 45 per cent of the strength to final rupture. Just before failure, at 95 per cent of strength, the rate increase is dropping, except for σ_x (Fig. 4b).

Sample CME24 was saturated at 91 per cent. The electrical conductivities slowly increase up to 34 per cent of strength, and then increase more rapidly, by 1.5–2 per cent for σ_x, σ_y and 3 per cent for σ_z up to failure. Before failure, at 91 per cent of strength the rate increase of the horizontal conductivities is dropping (Fig. 4c).

Sample CME23 was saturated at 87.6 per cent. The electrical conductivities first decrease by 0.5–0.7 up to 32 per cent of strength. Then the electrical conductivity increase up to failure, by 0.8 and 1.4 per cent for σ_y and σ_z, respectively, except for σ_x that decreases from 60 per cent of strength up to failure. Before failure, at 82 per cent of strength the rate increase in σ_y is dropping. Note that some σ_x data are missing, due to technical problems (Fig. 4d).

Sample CME13 was saturated at 85 per cent. The electrical conductivities first slowly increase up to 22 per cent of strength, then increase up to failure, by 3 per cent for σ_x and σ_y, and 4 per cent for σ_z. Before failure, at 95 per cent of strength, the rate increase of the horizontal conductivities is dropping (Fig. 4e).

Sample CME32 was saturated at 80 per cent. The electrical conductivities slowly increase up to 17 per cent of strength, and then increase more rapidly up to failure by 1–1.5 per cent, with a dropping in rate increase at 85 per cent of strength (Fig. 4f).

DISCUSSION

Electrical conductivity at various saturations (intact samples)

The resistivity of the samples roughly increases when water saturation is decreased, as shown in Fig. 3. This behaviour is consistent with the fact that the mineral grains act as an insulating matrix and conduction occurs solely through the pore fluid. The expression used to describe the variation of formation factor F with saturation S_w and porosity Φ is usually $F = \Phi^{-m} S_w^{-n}$ (Archie 1942). Since we compare different samples in Fig. 3, it may explain the roughly feature of the increase of formation factor with decreasing saturation. When the sample is fully saturated (sample CME21), the m-value deduced from this expression is 1 ± 0.2 (consistent with

Jouniaux *et al.* 1996), which is a low value for cementation exponent in carbonates (Focke & Munn 1985; Sen *et al.* 1997). The *n*-value deduced from the axial formation factor results (Fig. 3) is about 1, consistent with the observation that the *n*-value is close to the *m*-value (Waxman & Smits 1968). For the horizontal results, their dispersion does not allow us to derive a *n*-value. Especially the lower horizontal formation factor value at 80 per cent water saturation and the dispersion observed at 87.6 per cent saturation may be due to some heterogeneities in the horizontal lithology of the concerned samples.

Since our samples were saturated from 100 to 80 per cent, we may assume that we are not in the low-saturation regime where the conductivity involves surface conduction. In low-saturation regime, a dramatic decrease in resistivity occurs when saturation is increased, up to the presence of a few monolayers of water on the internal rock surfaces (Knight & Dvorkin 1992). These few monolayers of water correspond to water saturation of 4 to 10 per cent for the studied sandstones by Knight & Dvorkin (1992) and have been interpreted as the thickness of water layers for which the behaviour of water changes from that of a surface phase to that of a bulk phase (Knight & Dvorkin 1992). It can, therefore, be assumed that by using saturation between 80 and 100 per cent, the main mechanism involved in the conductivity will be the conductivity of bulk water.

Effect of uniaxial compression on the electrical conductivity of fully saturated sample (CME21)

When the rock is saturated, and in drained conditions, the axial electrical conductivity is thought first to decrease, and then to increase with compression. At the beginning of the deformation process, the closure of pores and subhorizontal cracks full of water induces a decrease in conducting paths and the conductivity of the rock decreases. Then, when new axial cracks form in the rock and when water is available, these cracks become new conducting paths, and the conductivity of the rock increases. This behaviour has been observed in triaxial experiments on crystalline rocks (Brace & Orange 1968), on Fontainebleau sandstone (Jouniaux *et al.* 1992), and on Darley Dale sandstone (Glover *et al.* 1997). It has been shown by Brace & Orange (1968) that the increase of conductivity begins about when the rock becomes dilatant and that a rapid increase in conductivity accompanies the rapid increase in volume. Most of the time the magnitude of conductivity increase is much more larger than the magnitude of conductivity decrease. This is not the case in our experiments, maybe because in uniaxial compression tests, the crack closure at low stress, which leads to a decrease in conductivity when in drained conditions, is more important than in triaxial compression tests, where the hydrostatic stress applied to the sample prior to triaxial testing has already partly closed the initial cracks.

In our study, measurements on CME21 sample which was fully saturated, show first a decrease and then an increase in horizontal conductivities, as expected for the axial conductivity. Note that the horizontal conductivity of a granite sample under triaxial deformation increased too (Brace & Orange 1968). However, the behaviour of the axial conductivity is more complex with an unusual transient increase at about 70 per cent of strength, roughly corresponding to the local minimum in the horizontal conductivity curves. Indeed in our uniaxial undrained experiments the sample is not connected to a water reservoir as it is usually the case in triaxial experiments, so that the available water volume is only the initial water volume present in the rock. The transient vertical conductivity increase may thus be explained by the differential closure of subhorizontal cracks

with their water content being expelled into the opening vertical cracks. The following light decrease may then be due to a transient lack of water in the new axial cracks forming in the sample. Further closing of subhorizontal cracks leads to the increase of water saturation in axial cracks resulting, when combined to their coalescence, in the increase in axial conductivity and the decrease in horizontal conductivities at failure.

The increase rate of axial conductivity from 40 to 70 per cent of strength is 0.13 per cent/MPa, of the same order as the one observed by Brace & Orange (1968) on Pottsville sandstone (0.14 per cent/MPa), and lies between the values obtained by Glover *et al.* (1997) on Darley Dale sandstone (0.06 per cent/MPa) and those measured by Jouniaux *et al.* (1992) on Fontainebleau sandstone (0.2 to 0.6 per cent/MPa). At failure, the 2 per cent increase in the axial conductivity and the decrease in horizontal conductivities confirm the subverticality of the final macroscopic fracture.

The conductivity increase is usually related to the crack porosity Φ_c, corresponding to new formed cracks, which is the difference between the actual volume change and the elastic volume change. The conductivity through cracks σ_c, which is obtained by subtracting crack-free conductivity (that would be the linear decrease of the conductivity from the beginning of the compression test, Fig. 5(a): straight line) from total conductivity (the measured conductivity, Fig. 5(a): empty squares), was calculated and compared to the crack porosity by Brace & Orange (1968). These authors showed that the crack conductivity was proportional to the crack porosity, so that $\sigma_c/\sigma_f = \Phi_c^m$ with $m = 1$ for their studied crystalline rocks, whereas for the Pottsville sandstone $m = 2$. The *m*-value, deduced from two independent measurements (volume change and conductivity
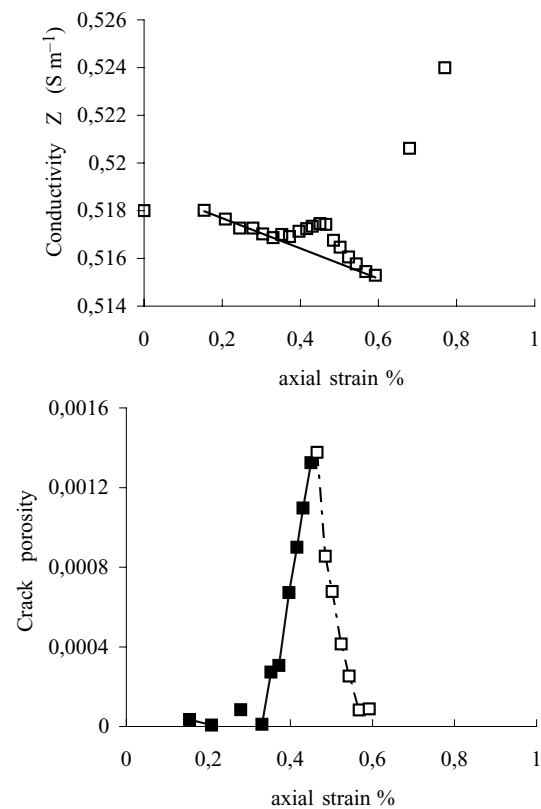

Figure 5. (a) Measured axial conductivity and the linear decrease of conductivity during the compression phase, for CME21 sample. (b) Crack porosity Φ_c during compression, deduced from $\sigma_c/\sigma_f = \Phi_c^m$ with $m = 1$.

change), was shown to be constant during compression up to the failure (Brace & Orange 1968). The same approach has been used by Glover *et al.* (1996), who assumed a *m*-value equal to 2 to compute a damage parameter which is the crack porosity. The crack porosity Φ_c has been computed for CME21 sample (Fig. 5b), with the *m*-value deduced from the measurements of porosity and formation factor before the deformation test ($m = 1$), and assuming that this *m*-value is constant during compression, as shown by Brace & Orange (1968). It can be seen that the crack porosity starts to increase at 0.33 per cent of axial strain, meaning 31 per cent of strength, and increases up to 0.46 per cent of strain (68 per cent of strength). When the rock is saturated, the conductivity change can, therefore, be related to the crack porosity and according to this analysis, the compression of the sample leads first to a decrease in volume, and then to a volume increase up to 68 per cent of strength. As noted previously a partial desaturation of new forming cracks may happen leading to a transient decrease of axial conductivity and, therefore, a transient decrease of the deduced crack porosity (Fig. 5b, dotted-line), before their drastic increase as failure approaches.

Since the cracks induced by the deformation are created in the axial direction, this analysis is not suitable for horizontal electrical measurements. Moreover, note that the crack porosity is related to the electrical conductivity change only if the cracks are filled with water, which is not the case for the following not-fully saturated conditions.

Effect of water saturation on the electrical conductivity behaviour during uniaxial compression tests

The largest variation in electrical conductivity during compression is usually in the axial direction (except for CME23 sample), in accordance to the fact that cracks are created in the axial direction during these uniaxial experiments. There is no obvious relation between the amplitude of conductivity increase and the water saturation, at least for the studied saturation range. When the water saturation is decreased, the electrical conductivity increase occurs earlier during compression (Fig. 6), so that the decrease in conductivity at low stress is less and less present (except for CME23 sample). The increase in conductivity occurs at 68, 50, 34, 32, 22 and 17 per cent of strength (see Fig. 4) for the decreasing saturations of 100, 95, 91, 87.6, 85 and 80 per cent, respectively. In order to compare the mechanical behaviour of the different samples, the axial stress has been plotted versus the axial strain on a single graph for the six studied samples (Fig. 7). The samples show a similar mechanical behaviour, except sample CME24 which shows a rather compliant initial behaviour maybe due to the presence of subhorizontal flaws. Therefore, the differences in the electrical conductivity variation during the compression will not be attributed to a possible mechanical difference, except possibly for the sample CME24.

Previous experiments on sedimentary rocks of high porosity (40–55 per cent) under uniaxial compression at various water saturation from 2 to 25 per cent showed an increase in electrical conductivity with stress (Yamazaki 1965; 1966). The conductivity increase was 0.5 per cent on lapilli tuff at 25 per cent water saturation, 2.5 per cent on tuffaceous sandstone at 9.5 per cent of water saturation; and 1 per cent on pumice tuff at 5.6 per cent of water saturation. When the initial water saturation was increased from 2 to 25 per cent in lapilli tuff samples, the magnitude of conductivity increase during the uniaxial compression tests dropped from 11 to 0.5 per
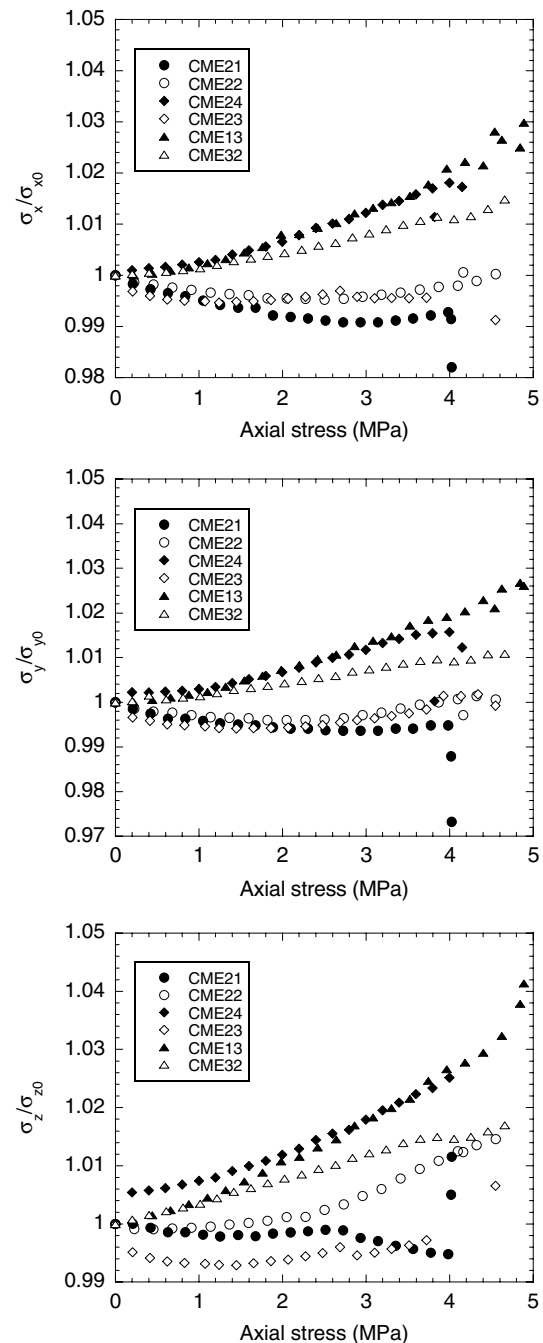

Figure 6. Rock conductivity versus axial stress for the six studied samples.

cent (Yamazaki 1966). As already mentioned by Brace & Orange (1968), when the rock is partially saturated, water films form only a partial network in the rock, and at low stress when cracks and pores are closed and porosity reduced, the connectivity of these films is increased. So that the initial conductivity is small and then increases with stress. Note that only a small water amount is needed to form a connected path throughout the sample, as low as one-fifth of a monolayer of water on the internal rock surfaces, corresponding to water saturation below 1 per cent for the sandstones studied by Knight & Dvorkin (1992).

However, the exact quantification of the involved processes both during the compression and in non-saturated and undrained conditions is hardly feasible. Some modelling exists that explains
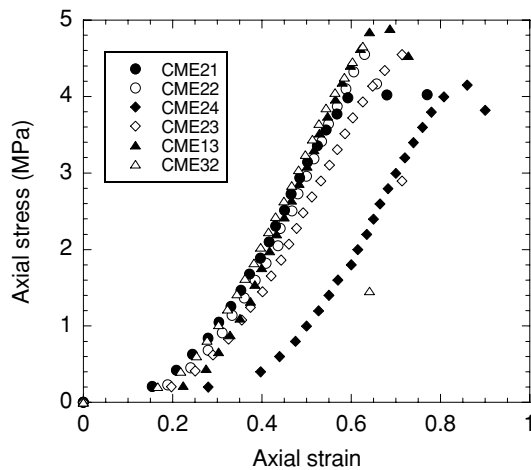
Figure 7. Axial stress versus axial strain for the six studied samples.

is observed for the second group (lower water saturation) (Figs 4 and 6).

When stress is further increased the electrical conductivity of partially saturated rocks increases, both in axial and horizontal directions. This increase occurs earlier during the compression process when the initial water saturation is lower (Figs 4 and 6). During dilatancy the porosity increases and the saturation decreases, so that the two terms in the equation of the conductivity variation are still in competition. The result of these competing effects shows that the connected path of water is eventually enhanced, both in the axial and horizontal directions (Fig. 6).

We finally plot the logarithm of the rock conductivity versus the axial stress (Fig. 8) in order to quantify the effect of stress on the
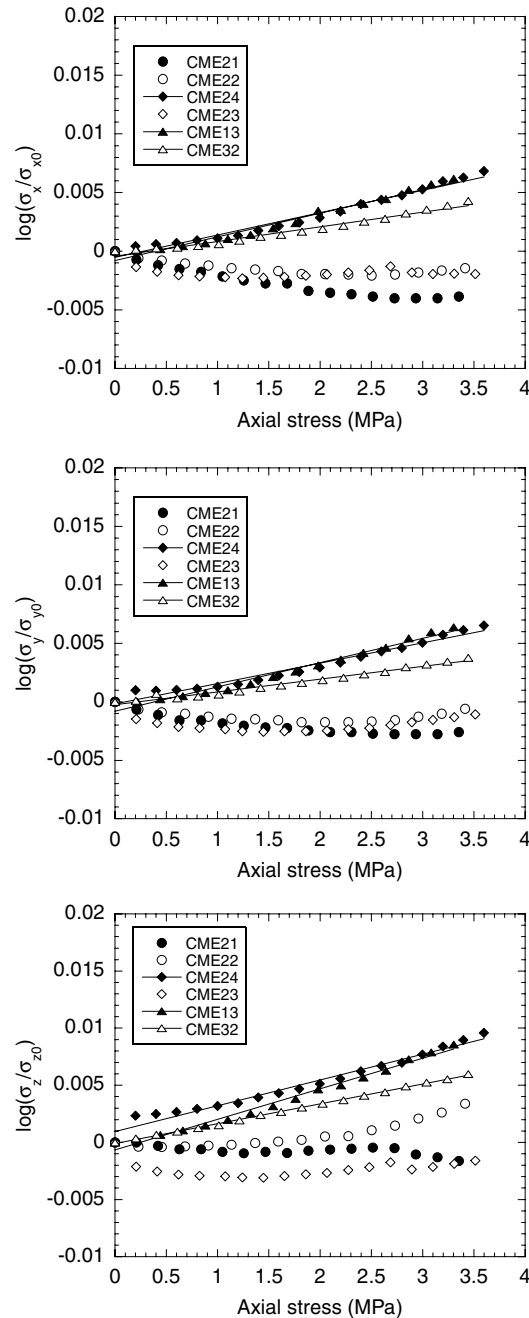
the decrease of electrical conductivity during the drainage of samples, leading to a decrease in water saturation, but without any deformation (see e.g. Brovelli *et al.* 2005). Other modelling exists that explains the effect of stress (P), in hydrostatic conditions and in saturated and drained conditions, on the electrical conductivity (Kaselow & Shapiro 2004). From Archie's law in saturated conditions $F = \Phi^{-m}$, these authors deduced a variation of the rock electrical conductivity σ_r as $\log(\sigma_f/\sigma_r) = A + KP - B\exp(-DP)$, the coefficients A, K, B, and D being fitting parameters for a given set of measurements. The first and second terms are related to the variation of the stiff porosity, and the last term is related to the compliant porosity. Note that in our case the pressure is the axial stress and not the hydrostatic pressure. From Fig. 6 it seems that the behaviour of the samples can be split into two groups: for the first group corresponding to samples with higher water saturation values (100, 95 and 87.6 per cent, meaning samples CME21, CME22, and CME23) the electrical conductivity decreases during the compaction phase before increasing at higher stress values, for the second group corresponding to lower water saturation values (85 and 80 per cent, meaning CME13 and CME32) the electrical conductivity increases from the beginning of the compression, the sample CME24 may be not comparable because of its different initial mechanical behaviour (Fig. 7).

In our case we should consider Archie's law in unsaturated conditions (see above). The induced relative variation of the rock conductivity is given by:

$$\frac{\delta\sigma_r}{\sigma_r} = \frac{\delta\sigma_f}{\sigma_f} + m\frac{\delta\Phi}{\Phi} + n\frac{\delta S_w}{S_w}$$

Water conductivity σ_f being constant, the first term is equal to zero. We can, therefore, see that two competing effects are present in non-saturated and undrained conditions: the relative variations of porosity Φ and saturation S_w during compression.

At low stress, when the rock volume is decreasing and pores or subhorizontal cracks are closing, the saturation is increasing since the water volume is constant. The water is expelled from closing cracks and distributed in the still open porous network. At this stage, the porosity decreases (the second term is negative) and the saturation increases (the last term is positive). The result of these competing effects depends on the initial saturation: a small decrease or almost constant axial and horizontal conductivity is observed for the first group of samples (higher water saturation), a small increase

Figure 8. Logarithm of the rock conductivity versus axial stress for the six studied samples.

evolution of rock conductivity in a similar way as that followed by Kaselow & Shapiro (2004). This analysis is done before the dilatancy onset at about 3.5 MPa (Fig. 7) to only take into account the initial crack population.

For highly saturated samples CME21 (100 per cent) and CME22 (95 per cent) the variation of the logarithm of the conductivity is not a straight line, neither for CME23 sample. On the contrary, for lower saturation, that is for samples CME32 (80 per cent), CME13 (85 per cent) and CME24 (91 per cent), a linear relationship exists in the axial (z) direction between the logarithm of the rock conductivity and stress with a slope of 0.0017, 0.0027 and 0.0023 MPa^{-1}, respectively, confirming that there is no clear relation between the amplitude of electric conductivity variation during compression and the initial water saturation value, at least in the studied range. In the horizontal directions, the slopes are 0.0011, 0.002, 0.0017 (in y direction), and 0.0013, 0.002 and 0.0019 (in x direction) for samples CME32, CME13 and CME24, respectively. The slope is, therefore, about 35 per cent larger in axial direction than in the horizontal directions, which is consistent with the fact that cracks are created in the axial direction. Moreover, note that in undrained and non-saturated conditions, the linear relationship observed between log σ_r and stress means that the relative increase in the electrical conductivity is larger as one goes along the compression.

Evolution of the anisotropy of electrical conductivity during compression

The plots of the electrical conductivity anisotropy (Fig. 4) show that there is no anisotropy in the radial plane. The anisotropy between axial and radial directions is larger, about 1 to 4 per cent, because during compression new cracks are created in the axial direction. We note that there is usually a continuous small increase in the anisotropy between axial and radial directions during the compression test, except the transient decrease in sample CME21. It results that the anisotropy between axial and radial directions is about 0.5–2 per cent just before failure. At failure a drastic increase of this anisotropy can be seen, up to 5–6 per cent (CME21, CME24 and CME13 samples).

CONCLUSION

When the rock is fully saturated the electrical conductivity first decreases, and then increases during the uniaxial compression test. Although our experiments are performed on highly porous sedimentary rocks, the magnitude of the rock conductivity variation is of the same order, meaning 1–4 per cent, as the one measured usually on granite or sandstone, and most of the time under triaxial deformation. We show that when saturation is decreased the conductivity increase occurs earlier in the compression process, from 68 to 17 per cent of strength for 100 to 80 per cent of water saturation, respectively. Therefore, the decrease in conductivity at low stress is less and less present. Continuous increase of electrical conductivity due to compression is measured as soon as the saturation is decreased to 85 per cent. For low saturation levels such as 80–85 per cent, the compression phase leads to an increase in axial conductivity, roughly following a power-law $\sigma_r \sim 10^{0.002P}$, where P is the axial stress in MPa. It is usually suggested to interpret the field observations of pre-seismic change in crustal resistivity in the light of laboratory measurements performed in saturated conditions. Although an upscaling of laboratory measurements to *in situ* measurements

is not simple, we suggest that *a continuous increase* of electrical conductivity due to compression should be probably expected as soon as the rocks are not fully saturated. These non-saturated conditions are more representative of the shallow crust. However at the scale of the sample the electrical conductivity increase is only about 1–4 per cent. Moreover a drastic increase in the anisotropy of electrical conductivity at fracture could be expected, and at the scale of the sample the anisotropy between axial and radial directions can be observed up to 5–6 per cent at rupture.

REFERENCES

Archie, G.E., 1942. The electrical resistivity log as an aid in determining some reservoir characteristics, *Trans. Am. Inst. Min. Meta. & Petrol.. Eng.,* **146,** 54–67.

Ashby, M.F. & Sammis, C.G., 1990. The damage mechanics of brittle solids in compression, *Pure appl. Geophys.,* **133,** 489–521.

Bernabé, Y., 1986. Pore volume and transport properties changes during pressure cycling of several crystalline rocks, *Mech. Mater.,* **5,** 235–249.

Bernabé, Y., 1995. The transport properties of networks of cracks and pores, *J. geophys. Res.,* **100,** 4231–4241.

Brace, W.F., 1975. Dilatancy-related electrical resistivity changes in rocks, *Pure appl. Geophys.,* **113,** 207–217.

Brace, W.F., 1980. Permeability of crystalline and argillaceaous rocks, *Inter. J. Rock Mech. Min. Sci. Geomech. Abst.,* **17,** 241–251.

Brace, W.F. & Orange, A.S., 1968. Electrical resistivity changes in saturated rocks during frature and frictional sliding, *J. geophys. Res.,* **73,** 1433–1445.

Brace, W.F., Paulding, B.W. & Scholz, C., 1966. Dilatancy in the fracture of crystalline rocks, *J. geophys. Res.,* **71,** 3939–3953.

Brovelli, A., Cassiani, G., Dalla, E., Bergamini, F., Pitea, D. & Binley, A.M., 2005. Electrical properties of partially saturated sandstones: novel computational approach with hydrogeophysical applications, *Water Resour. Res.,* **41,** W08411, doi:10.1029/2004WR003628.

Cornet, F.H., Doan, M.L. & Fontbonne, F., 2003. Electrical imaging and hydraulic testing for a complete stress determination, *Int. J. Rock Mech. Min. Sci.,* **40,** 1225–1241,.

David, C., Darot, M. & Jeanette, D., 1993. Pore structures and transport properties of sandstone, *Transp. Porous Media,* **11,** 161–177.

David, C., Menendez, B. & Darot, M., 1999. Influence of stress-induced and thermal cracking on physical properties and microstructure of La Peyratte granite, *Int. J. Rock Mech. Min. Sci.,* **36,** 433–448.

Eberhart-Philipps, D., Stanley, W.D., Rodriguez, B.D. & Lutter, W.L., 1995. Surface seismic and electrical methods to detect fluids related to faulting, *J. geophys. Res.,* **100,** 12 919–12 936.

Focke, J.W. & Munn, D., 1985. Cementation exponents in Middle Eastern carbonate reservoirs, presented at Middle Eastern Oil Show, Bahrain, Soc; Pet. Eng., *Pap. SPE 13735,* 431–442.

Fonseka, G.M., Murell, S.A.F. & Barnes, P., 1985. Scanning electron microscope and acoustic emission studies of crack development in rocks, *Int. J. Rock Mech. Min. Sci. & Geomech. Abstr.,* **22,** 273–289.

Glover, P.W.J., Gomez, J.B., Meredith, P.G., Boon, S.A., Sammonds, P.R. & Murrel, S.A.F., 1996. Modelling the stress-strain behavior of saturated rocks undergoing triaxial deformation using complex electrical conductivity measurements, *Surv. Geophys.,* **17,** 307–330.

Glover, P.W.J., Gomez, J.B., Meredith, P.G., Hayashi, K., Sammonds, P.R. & Murrel, S.A.F., 1997. Damage of saturated rocks undergoing triaxial deformation using complex electrical conductivity measurements: experimental results, *Phys. Chem. Earth,* **22,** 57–61.

Glover, P.W.J., Gomez, J.B. & Meredith, P.G., 2000. Fracturing in saturated rocks undergoing triaxial deformation using complex electrical conductivity measurements: Experimental study, *Earth planet. Sci. Lett.,* **183,** 201–213.

Guichet, X., Jouniaux, L. & Pozzi, J.P., 2003. Streaming potential of as and column in partial saturations conditions, *J. geophys. Res.,* **108,** 2141, doi:10.1029/2001JB001517.

Henry, P., Jouniaux, L., Screaton, E.J., Hunze, S. & Saffer, D.M., 2003. Anisotropy of electrical conductivity record of initial strain at the toe ofthe Nankai accretionary wedge, *J. geophys. Res.,* **108,** 2407, doi:10.1029/2002JB002287.

Hyndman, R.D. & Hyndman, D.W., 1968. Water saturation and high electricalconductivity in the lower continental crust, *Earth planet. Sci. Lett.,* **4,** 427–432.

Hyndman, R.D. & Shearer, P.M., 1989. Water in the lower continental crust: modelling magnetotelluric and seismic reflection results, *Geophys. J. Int.,* **98,** 343–365.

Jouniaux, L., Pozzi, J.P., Brochot, M. & Philippe, C., 1992. Resistivity changes induced by triaxial compression in saturated sandstones from Fontainebleau (France), *C. R. Acad. Sci. Paris,* **315,** Série II, p. 1493–1499.

Jouniaux, L., Lallemant, S. & Pozzi, J.P., 1994. Changes in the permeability, streaming potential and resistivity of a claystone from theNankai prism under stress, *Geophys. Res. Lett.,* **21,** 149–152.

Jouniaux, L., Dubet, L., Zamora, M. & Morat P., 1996. Physical properties of limestone from the quarry of Mériel, *C. R. Acad. Sci. Paris,* **322,** série IIa, 361–367.

Jouniaux, L., Pozzi, J.P., Berthier, J. & Massé, P., 1999. Detectionoffluid flow variations at the Nankai Trough by electric and magnetic measurements in boreholes or at the seafloor, *J. geophys. Res.,* **104,** 29 293–29 309.

Kaselow, A. & Shapiro, S.A., 2004. Stress sensitivity of elastic moduli and electrical resistivity in porous rocks, *J. Geophys. Eng.,* **1,** 1–11.

Knight, R. & Dvorkin, J., 1992. Seismic and electrical properties of sandstones at low saturations, *J. geophys. Res.,* **97,** 17 425–17 432.

Knight, R. & Endres, A., 1990. A new concept in modeling the dielectricresponse of sandstones: defining a wetted rock and bulk water system, *Geophysics,* **55,** 586–594.

Le Pennec, J.-L. *et al.*, 2001. Electrical conductivity and pore-space topology of Merapi lavas: implications for the degassing of porphyritic andesite magmas, *Geophys. Res. Lett.,* **28,** 4283–4286.

Lockner, D.A. & Byerlee, J.D., 1986. Changes in complex resistivity during creep in granite, *Pure appl. Geophys.,* **124,** 659–676.

Marquis, G. & Hyndman, R.D., 1992. Geophysical support for aqueous fluids in the deep crust: seismic and electrical relationships, *Geophys. J. Int.,* **110,** 91–105.

Morat, P. & Le Mouël, J.L., 1992. Signaux électrique sengendrés par des variations de contrainte dans des roches poreuses nonsaturées, *C. R. Acad. Sci. Paris,* **315,** Série II, 955–963.

Morat, P., Le Mouël, J.L., Nover, G. & Will, G., 1992. Variation annuelle de la saturation d'une roche de grande porosité induite par la variation saisonnière de la température extérieure et mesurée par voie électrique, *C. R. Acad. Sci. Paris,* **315,** Série II, 1083–1092.

Nesbitt, B.E., 1993. Electrical resistivities of crustal fluids, *J. geophys. Res.,* **98,** 4301–4310.

Nover, G., Heikamp, S. & Freund, D., 2000. Electrical Impedance Spectroscopy used as a tool for the detection of fractures in rock samples exposed to either hydrostatic or triaxial pressure conditions, *Nat. Hazards,* **21,** 317–330.

Olhoeft, G.R., 1981. Electrical properties of granite with implications forthe lower crust, *J. geophys. Res.,* **86,** 931–936.

Parkhomenko, E.I. & Bondarenko, A.T., 1960. Effect of unilateral pressure on electrical resistance of rocks, Bull. Acad. Sci. USSR, *Geophysics Ser.,* **2,** 214–219 (English version).

Pezard, P., 1990. Electrical properties of Mid-Ocean ridge basalt and implications for the structure of the upper oceanic crust in Hole 504B, *J. geophys. Res.,* **95,** 9237–9264.

Scholz, C.H., Sykes, L.R. & Aggarwal, Y.P., 1973. Earthquake prediction: a physical basis, *Science,* **181,** 803–810.

Sen, P.N., Kenyon, W.E., Takezaki, H. & Petricola, M.J., 1997. Formation factor of carbonate rocks with microporosity: model calculations, *J. Petroleum Science and Engineering,* **17,** 345–352.

Takano, M., Yamada, I. & Fukao, Y., 1993. Anomalous electrical, resistivity of almost dry marble and granite under axial compression, *J. Phys. Earth,* **41,** 337–346.

Tapponier, P. & Brace, W.F., 1976. Development of stress-Inducedmicrocracks in Westerly granite, *Int. J. Rock Mech. Min. Sci. Geomech. Abstr.,* **13,** 103–112.

Thouret, L.R. & Marquis, G., 1994. Deep fluids and electrical conductivity of the lower continental crust, *C.R. Acad. Sci. Paris,* **318,** Ser. II, 1469–1482.

Waxman, M.H. & Smits, L.J.M., 1968. Electrical conductivities in oil-bearing shaly sands, *Trans. AMIE,* **243,** 107–122.

Wong, T.-f., 1982. Micromechanics of faulting in Westerly granite, *Int. J. Rock Mech. Min. Sci. Geomech. Abstr.,* **19,** 49–64.

Yamazaki, Y., 1965. Electrical conductivity of strained rocks, laboratory experiments on sedimentary rocks, *Bull. Earthquake Research Institute,* **43,** 783–802.

Yamazaki, Y., 1966. Electrical conductivity of strained rocks, further experiments on sedimentary rocks, *Bull. Earthquake Research Institute,* **44,** 1553–1570.